Optical and Quantum Electronics (2022) 54:463
https://doi.org/10.1007/s11082-022-03838-x

Optical absorption engineering in two-dimensional quantum rings: design and optimization for FIR to MIR detection applications

Mahdi Solaimani[1] · Alireza Mobini[2] · Abdolreza Rasouli Kenari[3]

Received: 9 February 2022 / Accepted: 21 May 2022 / Published online: 22 June 2022

Abstract
In this work, we present the new photodetector based on snowflake quantum rings (QRs) structure utilizing a two-dimensional tight-binding model. Optical absorption has calculated and compared with different usual geometries of rectangular, triangular and circular QRs. There are narrow dominant peaks in the absorption spectrum with a low FHWM of 15 meV in the range of 50 meV in the far-infrared (FIR) regime to 300 meV in the mid-infrared (FIR) regime. The two-dimensional confining potential for Koch shaped quantum ring had been described in previous work was inserted in the tight-binding method and probability density of nine lowest electron energy states and absorption have calculated for the first time. Using these results, some properties of QRs were predicted and their validity was examined and displayed further. For a Koch shape quantum ring, there is fine displacement about 3 meV in absorption peak in long-wavelength infrared regime with changing iteration number that can be used for fine-tuning of the absorption spectrum. Also, a circular ring with minimal energy states has absorption peaks with an average full width at half maximum of 12.5 meV that can be tuned with the resolution of 13 meV in the FIR regime. These results are more applicable for an experimentalist to design a new photodetector with a narrower sharp peak for applications like night-vision, a thermal detector, and total IR absorbers.

Keywords Snowflake quantum rings · Tight-binding model · Photodetector · FIR · LWIR · MIR

✉ Alireza Mobini
ar.mobini@iau-tnb.ac.ir; ar_mobini2009@yahoo.com

[1] Department of Physics, Qom University of Technology, Qom, Iran

[2] Department of Electrical and Computer Engineering, Islamic Azad University Tehran North Branch, Tehran, Iran

[3] Department of Electrical and Computer Engineering, Qom University of Technology, Qom, Iran

1 Introduction

Quantum rings (QRs) are a variant of toroidal-shaped quantum dot systems within them the number of confined electrons or holes can be managed to obtain many electronic and optical properties (Solaimani and Mobini 2020; Zozulenko et al. 1995; Mobini and Ahmadi 2014; Mohammad ghasemi et al. 2016; Lu et al. 2007). These properties lead to optical emission and absorption in the IR regime that has interesting scientific and industrial applications (Mohammad ghasemi et al. 2016; Lu et al. 2007; Billaha and Das 2016; Palaferri et al. 2018; Meng et al. 2014; Cheng et al. 2015; Li et al. 2015). These characteristics, make QRs highly promising candidates for the elegant fabrication of optoelectronic devices. These nanoscopic QRs can be fabricated by different techniques such as self-assembly (Lee et al. 2006) or lithographic (Bayer et al. 2003), as described in experimental works (Lorke et al. 2000; Warburton et al. 2000; Kong et al. 2004; He et al. 2010; Strom et al. 2007; Wang and Vasilopoulos 2007; Emperador et al. 1999; Bagraev et al. 2008; Garcia et al. 2004). Different shapes of quantum ring systems such as quantum dot rings (Hedin and Joe 2011), the array of mesoscopic rings (Dutta et al. 2010), ring superlattices (Nunnenkamp et al. 2008), vertically stacked QRs (Szafran et al. 2007), limaçon-shaped ring (Bruno-Alfonso and Latgé 2008), etc. have so far been reported and different properties of QRs have been investigated. Studying the transition energies and oscillator strengths of excitons in dependence on magnetic field in coaxial and non-coaxial nanorings (Grochol et al. 2007), Aharonov-Bohm effect in concentric quantum double rings (Chen et al. 2007), optical Aharonov-Bohm effect in volcano shaped GaAs ring (Li and Peeters 2011), electron escape rate in a concentric circular mesoscopic ring (Tomita and Suzuki 1996), landau quantization in a concentric circular ring (Tan and Inkson 1996), Berry phase in one-dimensional circular ring with an adiabatic rotating potential (Zhu 2000) and persistent current and magnetic susceptibility of disordered circular concentric QRs (Mikhailov et al. 2006) etc. have till now been explored. Among the physical properties of QRs, optical absorption have a special situation. There are different reasons to use QRs as an absorber: detection a wide range of wavelengths from IR to THZ (Dai et al. 2008; Ling et al. 2009; Ghafari et al. 2019), high performance QRs based detector for terahertz range (Bhowmick et al. 2010). In this way, the effects of electric field (Solaimani et al. 2013a, b), excitons (Govorov et al. 2002), Rashba effect (Splettstoesser et al. 2003) or Dresselhaus effect (Nita et al. 2012), spin–orbit coupling and also impurities (Baghramyan et al. 2014) can produce considerable changes in the electronic properties of the QRs. Optical absorption of two electron QRs (Solaimani et al. 2015), the effect of magnetic field with Bessel functions (Barticevic et al. 2000), the effect of parallel magnetic field (Nasri 2021) and impurity effects on the optical absorption of circular QRs (Dias da Silva et al. 2006), have been carefully studied.

All these studies have considered the specific shape of QR and the results for different shapes of QR have not compared yet. In the present study, we investigate the optical absorption coefficient of rectangular, triangular, circular, and new snowflake QRs for the first time. For this purpose, we solve the equations resulting from the two-dimensional tight-binding model to evaluate the physical properties of the system. Besides, we compare three other geometries of rectangular, triangular and circular ones with the snowflake geometry to find the extent of the tunability of these structures in different regime from LWIR to MIR.

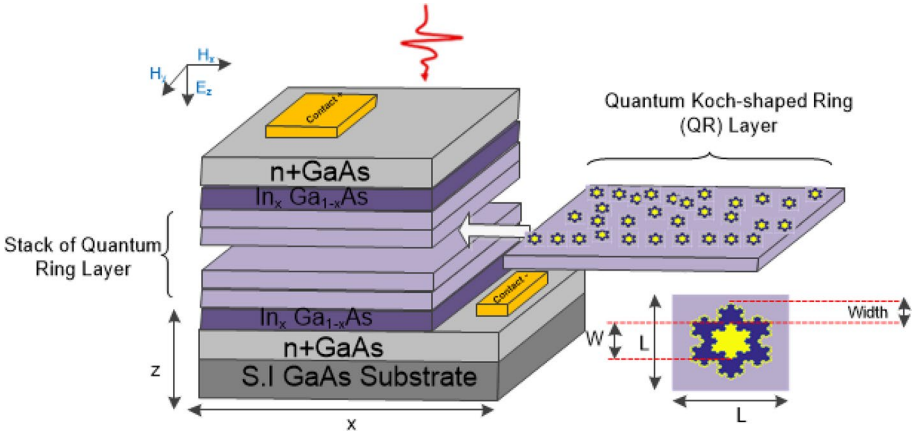

Fig. 1 Schematic of photodetector structure constructed from stacked quantum Koch-shaped ring layer

2 Structure and simulation theory

The schematic of the structure has been depicted in Fig. 1.As shown in this figure the active layer has constructed from stack of Koch-shaped QRs witch located between $In_xGa_{1-x}As$ and n + GaAs as ohmic layer.

The tight-binding model for an electron in a Nx × Ny two-dimensional square lattice can be written as (Zozulenko et al. 1995),

$$H = \sum_{m,n}^{N_x,N_y} \left(\varepsilon_0 + V_{nm}\right) c_{m,n}^{\dagger} c_{m,n} - t \sum_{m,n}^{N_x,N_y} \left\{ c_{m,n}^{\dagger} c_{m+1,n} + c_{m,n}^{\dagger} c_{m,n+1} \right\} + h.c \tag{1}$$

where m and n are some integers showing the x and y coordinates respectively. $c_{m,n}^{\dagger}\left(c_{m,n}\right)$ are electron creation (annihilation) operators at the site (m, n) and 't' is the hopping energy between the different sites. The potential profile V_{nm} has been numerically evaluated. Then, we can write (Solaimani et al. 2020; Zozulenko et al. 1995),

$$E\psi_{m,n} = \left(\varepsilon_0 + V_{nm}\right)\psi_{m,n} - t\psi_{m+1,n} - t\psi_{m,n+1} - t\psi_{m-1,n} - t\psi_{m,n-1} = H_{n,m} \tag{2}$$

where, $\psi_{m,n}$ is the Eigen-ket for the full Hamiltonian at a site (m, n). The Matrix H is $(N_x \times N_y) \times (N_y \times N_x)$. This matrix yields the following matrix eigenvalue problem problem (Solaimani et al. 2020; Zozulenko et al. 1995),

$$\left[\hat{H} - E_{n,j}\right]_{(N_x \times N_y) \times (N_x \times N_y)} \left[\psi_n\right]_{(N_x \times N_y) \times 1} = 0 \tag{3}$$

After diagonalization, the eigen-energies of the system will be obtained. Now, we study the absorption spectrum which can be defined as (Assuncao et al. 2011; Mobini and Solaimani 2018)

$$A(E) = \frac{1}{N} \sum\nolimits_{\beta} \delta\left(E - E_{\beta}\right) F_{\beta} \tag{4}$$

where E_β is the βth energy eigenvalue, $\delta(E - E_\beta)$ is the Dirac delta function, and F_β is the' oscillator strength associated with the eigenvalue β, i.e. (Assuncao et al. 2011; Mobini and Solaimani 2018):

$$F_\beta = \left[\sum_{n=1}^{N} \psi_n(E_\beta)\right]^2 \tag{5}$$

Here, $\psi(E_\beta)$ is the eigenfunction corresponds to the energy eigenvalue E_β.

3 Results and discussions

For this simulation, the two-dimensional QRs with different geometries such as rectangular, triangular, circular, and snowflake have been considered and the probability density of nine lowest electron energy states calculated utilizing a two-dimensional tight-binding model. In the first step, a triangular quantum ring made of GaAs/AlGaAs with L = 30 nm, W = 5 nm, Width = 5 nm has been considered. L is the length of external square, W is the length of internal square and width is the width of the ring as depicted in Fig. 1. Confining potential depth and electron effective mass for simulated material are adapted from references were shown in Table 1:

Probability density of nine lowest electron energy states for this structure are calculated and denoted in Fig. 2.

As seen in Fig. 2, A and F are the symmetric states. Utilizing the same method used for the triangular quantum ring, the probability density of nine lowest electron energy states of rectangular QRs with L = 30 nm, W = 5 nm, Width = 5 nm, have been calculated and depicted in Fig. 3 too. In this figure, the D and E are symmetric states. In the same way, the probability density of nine lowest electron energy states for Koch-shaped QRs and circular QRs have been calculated and depicted in Figs. 4 and 5, respectively. As seen in these figures, for Koch-shaped QRs, A, F and G are symmetric states and for circular QRs, except B and C states the remaining are symmetric states. So, because of this symmetry, it is expected that state energy for circular and Koch-shaped QRs be smaller than triangular and rectangular rings.

From comparison of probability destiny in Fig. 2–5, it is found that by using the proposed confining potentials, we can tune the position and intensity of the wave function in any part of the system. As we know, the wave function square is directly related to the distribution of the free carriers in the systems. Therefore, we can forwardly regulate the carrier distribution and finally inter-band absorption inside the system.

Now, we calculated the energy eigenvalues as a function of the energy level number for triangular, rectangular, Koch-shaped, and circular QRs. Figure 6 shows the variation of the energy eigenvalues as a function of the energy level index for triangular, rectangular, Koch-shaped, and circular QRs. As can be seen in this figure, there are some states with same energy. Considering Fig. 6 and previous Figs. 2–5, reveals that for the triangular, rectangular, snowflake-shaped and circular systems, some states are degenerate. However the circular system has shown in Fig. 5, has the maximum number of the degenerate states. This is because, the circular QRs have the maximum symmetry among the studied systems. In these figures, as the symmetry of the system increases, the number of degenerate states also increase. In Fig. 5, the states B and C, D and E, F and G as well H and I are degenerate states.

Table 1 Confining potential depth and electron effective mass have been used in this study

Material	m^*	V_{conf}(eV)
GaAs/ $Al_xGa_{1-x}As$	$0.067/(0.067+0.083x)m_0$ (Mobini and Solaimani 2018; Adachia 1985)	0.228 (Mobini and Solaimani 2018; Solaimani et al. 2013a, b)

Also as expected from Figs. 4 and 5, the energy states for Koch-shaped and circular QRs are less than other shapes. The minimum energy of circular and Koch-shape are 70 and 120 meV respectively but the minimum energy of other ring starts from 120 meV and finished at 330 meV. Also, it is interesting to note that, for the circular ring, the distance between energy bands is lower than other rings. It can be seen in Fig. 6. So, it is expected that absorption occurs in lower energies comparing to other rings with a larger distance in energy band (especially for the triangular ring).

To examine this idea, the absorption coefficient has been calculated as a function of the incident photon energy for different ring shapes. Also, the effect of structural parameters including widths and W investigated for each ring. The absorption coefficient for the triangular ring for L = 30 nm and their different values of width 5, 7.5, and 10 nm, Vconf = 300 meV were calculated and shown in Fig. 7. As seen in this figure, for the width of 10 nm, there are two narrow peaks in the absorption spectrum with FHWM of 13 meV almost in 57 and 214 meV. For a width of 7.5 nm absorption peaks moved to 83 and 282 meV and for the width of 5 nm absorption peaks moved to 133 meV respectively. When the width of the ring is decreased, the absorption peaks shift to higher energies. This blueshift expected because the size of the quantum ring is decreased and the energy level distances increase because of more quantum confinement.

In the same way, the absorption coefficient for the rectangular quantum ring with W = 5 nm and three different widths of 5, 10, and 15 nm has been calculated and depicted in Fig. 8.

As seen in this figure, the strongest peak is located in low energy and has a blue shift (from 34 to 132 meV) with decreasing width, same as before trending in the triangular ring. The second peak occurs in high energy and vanished when widths increased to 15 nm. Also, for this structure, the effect of changing W was examined on the absorption coefficient. As seen, for W of 5 nm, three strongest peaks in 34, 59, and 132 meV moved to 37, 66 and 138 meV for W of 10 nm and the weak peak vanished totally. Also, the FWHM increased from 13.2 meV to 15.1 when the width increased from 5 to 15 nm.

In the following, a similar simulation was done for Koch-shaped quantum ring form which captured from nature, and the absorption coefficient of this structure was calculated for the first time according to our knowledge. The absorption spectrum for a Koch-shaped quantum ring with L = 30 nm and different widths has been shown in Fig. 9.

For a quantum ring with a width of 10 nm, there are three peaks in 50, 141, and 254 meV with an average FWHM of 12.3 meV, that dominant peak occurs in 50 meV. As the width increases the peak amplitude increases and moves toward higher energy as discussed before.

Also, for a Koch-shaped quantum ring, there is a structural parameter known as the number of iterations that seems can affect absorption significantly. In this regard, we calculated and plotted the absorption vs Koch iteration number in Fig. 10.

According to this figure, for 1 iteration-based quantum ring with a width of 5 nm, absorption peaks occur at 121 (FWHM of 13 meV) and 288 meV (FWHM of 17 meV)

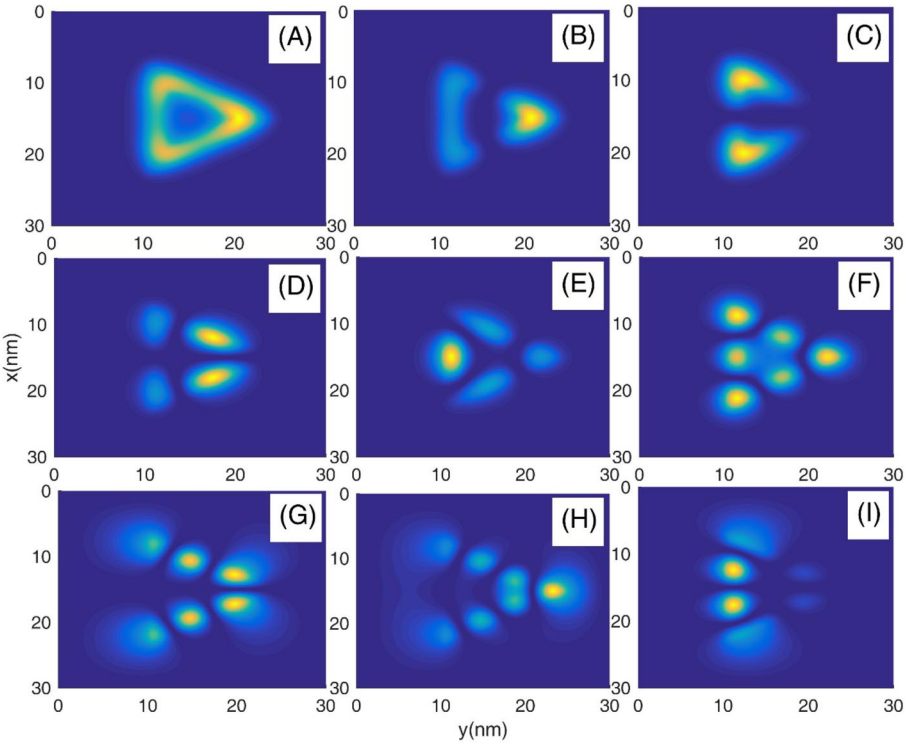

Fig. 2 Contour plots of probability density of nine lowest electron energy states of triangular QRs with L = 30 nm, W = 5 nm, Width = 5 nm

in the MIR regime. These peaks for a quantum ring with 2 iterations, moved to 119 (FWHM of 13 meV) and 276 meV (FWHM of 16.1 meV) which have little difference from their previous values. This redshift can be used for fine-tuning the absorption spectrum. A similar trend happens for the quantum ring with 3 iterations when related peaks move to 118 and 275 meV.

Finally, a circular quantum ring considered and the absorption coefficient as a function of incident photon energy has been calculated and indicated in Fig. 11.

The absorption has narrow dominant peaks in 27 (FWHM of 13.1 meV), 40 (FWHM of 12.6 meV), and 70 (FWHM of 14 meV) meV in FIR regime for different widths of 10, 7.5, and 5 nm, respectively. As predicted before, according to the result of Fig. 6, there is not absorption in higher energy for this ring because of the low distance between energy bands.

In last section of our study, we calculated and plotted the absorption spectrum for different values of V_{conf} as been depicted in the Fig. 12. In fact, the change of V_{conf} value is equivalent to the change of construction material of the QR. Comparing these figures, we can see for all QRs, absorption peak has blueshift with increasing V_{conf}, because the interval between conduction and valence band increases generally. For MIR regime, the absorption amplitude decreases with increasing $V_{conf,}$ but for lower energies in FIR regime, the absorption amplitude increases for all QRs. Also, the linear behavior can be seen in the absorption line starts from 100 meV with a minimum value of $V_{conf.}$

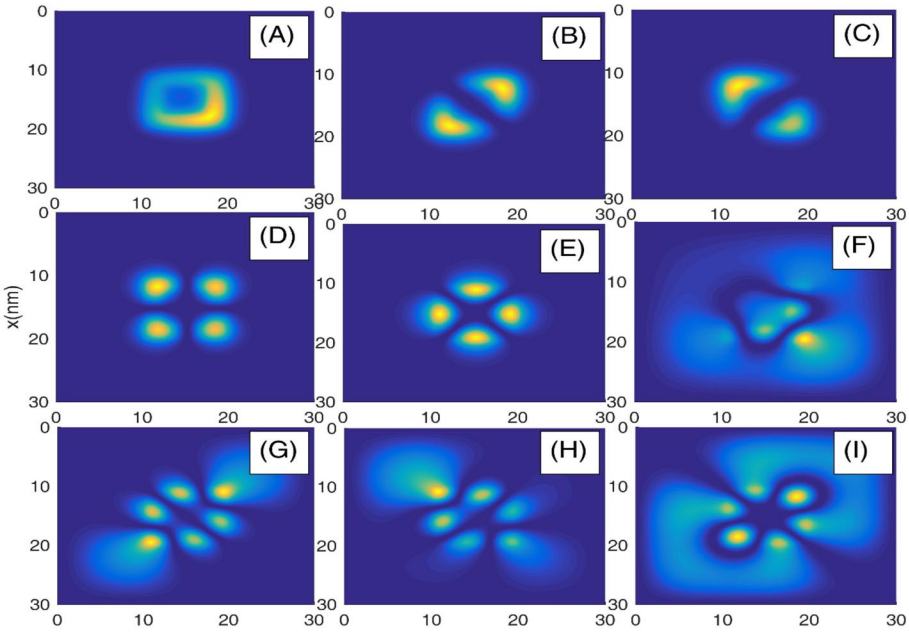

Fig. 3 Contour plots of probability density of nine lowest electron energy states of rectangular QRs with L = 30 nm, W = 5 nm, Width = 5 nm

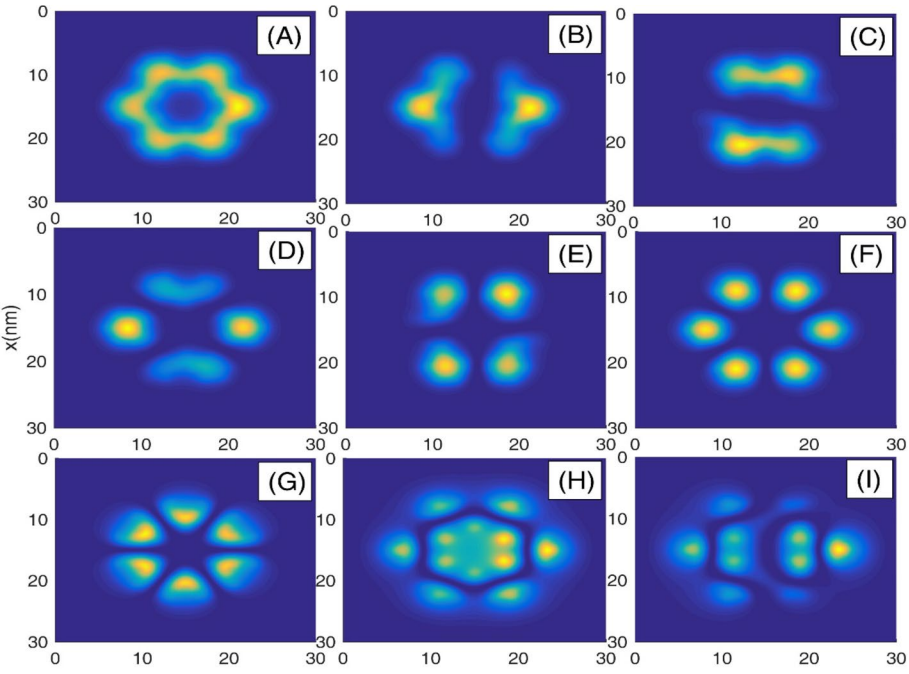

Fig. 4 Contour plots of probability density of nine lowest electron energy states of Koch-shaped QRs with L = 30 nm, W = 5 nm, Width = 5 nm

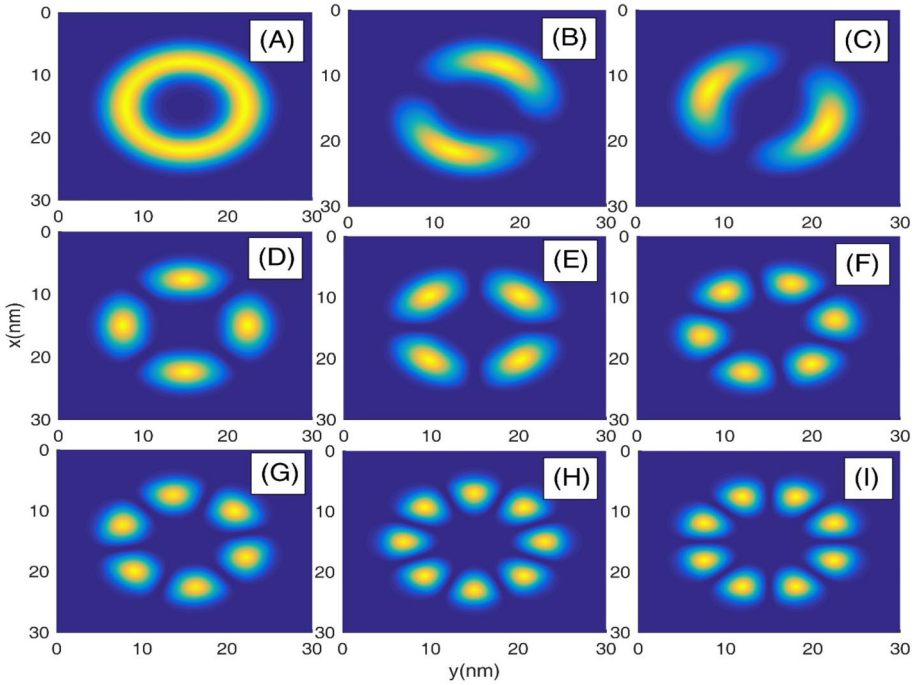

Fig. 5 Contour plots of probability density of nine lowest electron energy states of circular QRs with L = 30 nm, W = 5 nm, Width = 5 nm

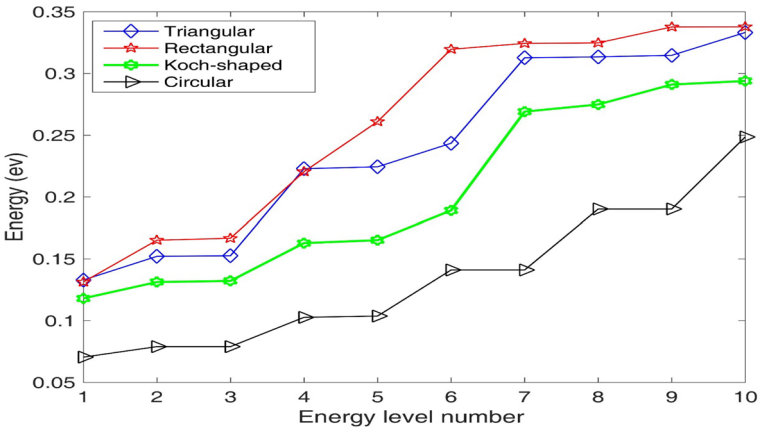

Fig. 6 Variation of the energy eigenvalues as a function of the energy level index for triangular, rectangular, Koch-shaped, and circular quantum ring

4 Conclusion

In summary, we used well know tight-binding method for calculating optical absorption of two-dimensional QRs with different geometries like rectangular, triangular, circular, and

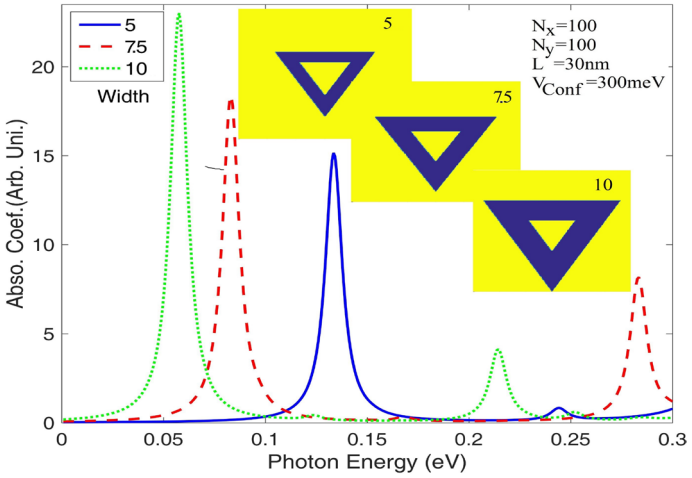

Fig. 7 Variation of the absorption coefficient as a function of the incident photon energy for three different ring width for triangular quantum ring

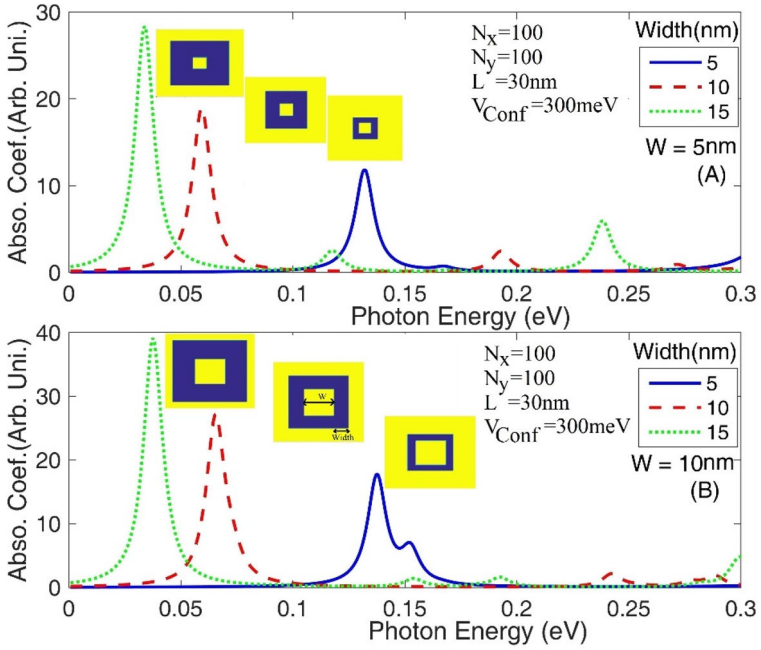

Fig. 8 Variation of the absorption coefficient as a function of the incident photon energy for three different ring width for rectangular quantum ring

snowflake. Some properties from probability densities and energy states are extracted and predicted and then verified by calculating the absorption spectrum. In Koch shape quantum ring with 1 iteration and with a width of 5 nm, narrow absorption peaks with HWFM of 15 meV occur at 121 and 288 meV. These peaks for a quantum ring with 2 iterations,

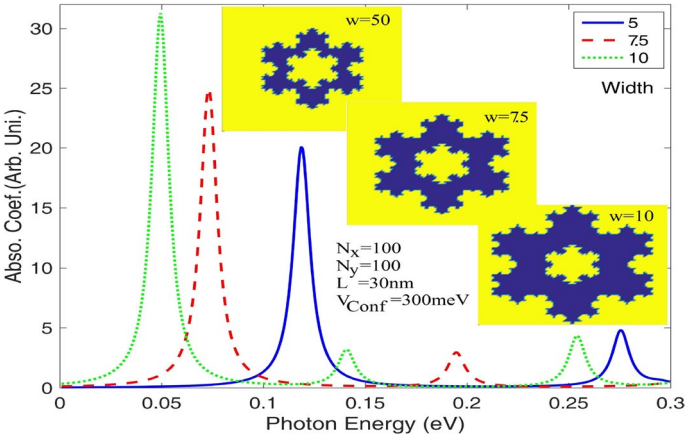

Fig. 9 Variation of the absorption coefficient as a function of the incident photon energy for three different ring width for snow-flake-shaped quantum ring

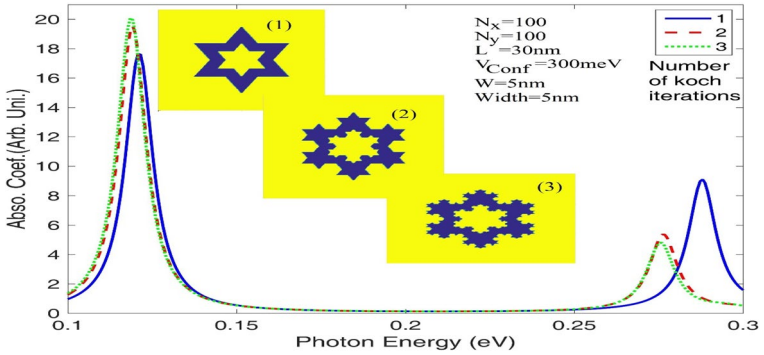

Fig. 10 Variation of the absorption coefficient as a function of the incident photon energy for three different Koch iteration numbers for snow-flake-shaped quantum ring

moved to 119 and 276 meV, which have little difference from their previous values. This redshift can be used for fine-tuning of absorption spectrum of Koch QRs. Also, there is a blue shift in absorption peaks with increasing the width for all QRs, because of quantum confinement. Furthermore, the effect of V_{conf} has investigated on absorption spectrum. We achieved that for all QRs, absorption peak has blueshift with increasing V_{conf}, and in MIR regime, the absorption amplitude decreases with increasing $V_{conf,}$ but for lower energies in FIR regime, the absorption amplitude increases. These structures and results can be used to design new enhanced nano-optical photodetector with high accuracy.

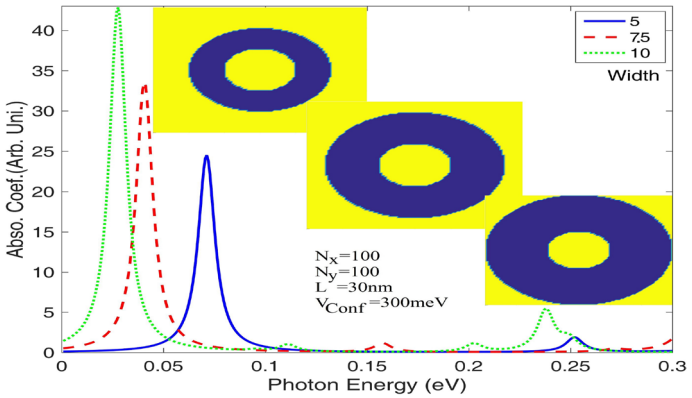

Fig. 11 Variation of the absorption coefficient as a function of the incident photon energy for three different ring width for circular quantum ring

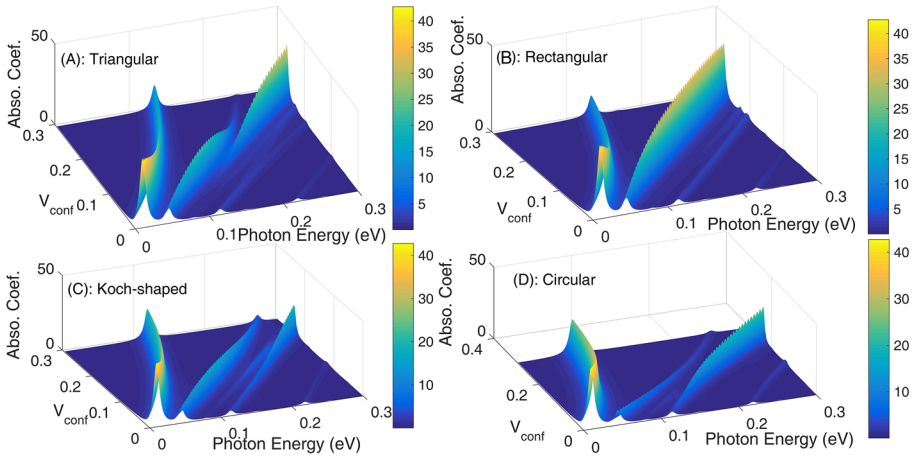

Fig. 12 **a** three-dimensional plot of the absorption coefficient as a function of the incident photon energy and confining potential depth Vconf for triangular QRs. **b** same as the panel (**a**) but for rectangular QRs. **c**: same as the panel (**a**) but for Koch-shaped QRs. **d** same as the panel (**a**) but for circular QRs

Funding There is no funding for this work.

Data availability All data that support the findings of this study are included within the article.

Declarations

Conflict of interest The authors declare no competing interests.

References

Adachia, S., GaAs, AlAs, AlxGa1−xAs: Material parameters for use in research and device applications. J. Appl. Phys. **58**(1) (1985)

Assuncao, T.F., Lyra, M.L., de Moura, F.A.B.F., Dominguez-Adame, F.: Coherent electronic dynamics and absorption spectra in an one-dimensional model with long-range correlated off-diagonal disorder. Phys. Lett. A **375**, 1048 (2011)
Baghramyan, H.M., Barseghyan, M.G., Kirakosyan, A.A., Restrepo, R.L., Mora-Ramos, M.E., Duque, C.A.: J. Lumin. **676**, 145 (2014)
Bagraev, N.T., Galkin, N.G., Gehlhoff, W., Klyachkin, L.E., Malyarenko, A.M.: J. Phys.: Condens. Matter **20**, 164202 (2008)
Barticevic, Z., Pacheco, M., Latge, A.: Quantum rings under magnetic fields: electronic and optical properties. Phys. Rev. B **62**, 6963 (2000)
Bayer, M., Korkusinski, M., Hawrylak, P., Gutbrod, T., Michel, M., Forchel, A.: Optical detection of the Aharonov–Bohm effect on a charged particle in a nanoscale quantum ring. Phys. Rev. Lett. **90**, 186801 (2003)
Bhowmick, S., Huang, G., Guo, W., Lee, C.S., Bhattacharya, P., Ariyawansa, G., Perera, A.G.U.: Appl. Phys. Lett. **96**, 231103 (2010)
Billaha, A., Das, M.K.: Influence of doping on the performance of GaAs/AlGaAs QWIP for long wavelength applications. Opto-Electron. Rev. **24**, 25–33 (2016)
Bruno-Alfonso, A., Latgé, A.: Quantum rings of arbitrary shape and non-uniform width in a threading magnetic field. Phys. Rev. B **77**, 205303 (2008)
Chen, G.-Y., Chen, Y.-N., Chuu, D.-S.: The Aharonov–Bohm effect in concentric quantum double rings. Solid State Commun. **143**, 515–518 (2007)
Cheng, Y., Luo, X., Song, J., Liow, T.-Y., Lo, G.-Q., Cao, Y., et al.: Passively mode-locked III-V/silicon laser with continuous-wave optical injection. Opt. Express **23**, 6392–6399 (2015)
Dai, J.H., Lee, J.H., Lin, Y.L., Lee, S.C.I.: Jpn. J. Appl. Phys. **47**, 2924 (2008)
Dias da Silva, L.G.G.V., Ulloa, S.E., Shahbazyan, T.V.: Impurity effects in the optical absorption of quantum rings. Physica E **32**, 37–40 (2006)
Dutta, P., Maiti, S.K., Karmakar, S.N.: Quantum transport in an array of mesoscopic rings: effect of interface geometry. Solid State Commun. **150**, 1056–1061 (2010)
Emperador, A., Barranco, M., Lipparini, E., Pi, M., Serra, L.: Phys. Rev. B 59 (1999)
Mohammad ghasemi, F., Ahmadi, V., Mobini, A.: Design and analysis of enhanced infrared photodetector based on plasmonic antenna with gold back-reflector. In: 2016 24th Iranian Conference on Electrical Engineering (ICEE), Shiraz, pp. 1170–1174. https://doi.org/10.1109/IranianCEE.2016.7585698 (2016)
Garcia, J. M., Granados, D., Silveira, J. P., Briones, F.: Microelectron. J. 35 (2004)
Ghafari, S., Mobini, A., Solimani, M.: Nano-scale planar photodetector based on ring form MQWs for FIR regime. JOSA B **36**(4), 897–900 (2019)
Govorov, A.O., Kalameitsev, A.V., Warburton, R., Karrai, K., Ulloa, S.E.: Physica E **13**, 297 (2002)
Grochol, M., Zimmermann, R.: Noncircular semiconductor nanorings of types I and II: emission kinetics in the excitonic Aharonov–Bohm effect. Phys. Rev. B **76**, 195326 (2007)
He, J.H., Chen, C.Y., Ho, C.H., Wang, C.W., Chen, M.J., Chen, L.J.: "Growth and structural characterization of SiGe nanorings. J. Phys. Chem. C **114**, 5727 (2010)
Hedin, E.R., Joe, Y.S.: Sensitive spin-polarization effects in an Aharonov–Bohm double quantum dot ring. J. Appl. Phys. **110**, 026107 (2011)
Kong, X.Y., Ding, Y., Yang, R., Wang, Z. L.: Science **303** (2004)
Lee, J.H., Mwang, Zh., Abuwaar, Z.Y., Strom, N.W., Salamo, G.J.: Evolution between self-assembled single and double ring-like nanostructures. Nanotechnology **17**, 3973–3976 (2006)
Li, B., Peeters, F.M.: Tunable optical Aharonov–Bohm effect in a semiconductor quantum ring. Phys. Rev. B **83**, 115448 (2011)
Li, X., Yu, X., Sun, Z., Yan, Z., Sun, B., Cheng, Y., et al.: High-power graphene mode-locked Tm/Ho co-doped fiber laser with evanescent field interaction. Sci. Rep. **5**, 16624 (2015)
Ling, H.S., Wang, S.Y., Lee, C.P., Lo, M.C.: J. Appl. Phys. **105**, 034504 (2009)
Lorke, A., Luyken, R.J., Govorov, A.O., Kotthaus, J.P.: Phys. Rev. Lett. 84 (2000).
Lu, J.-H., Wu, K.-J., Hsieh, K.-J., Kuan, C.-H., Feng, J.-Y., Lay, T.-S., et al.: A superlattice infrared photodetector integrated with multiple quantum wells to improve the performance. IEEE J. Quantum Electron. **43**, 72–77 (2007)
Meng, B., Tao, J., HuiLi, X., Quan Zeng, Y., Wu, S., Jie Wang, Q.: Tunable single-mode slot waveguide quantum cascade lasers. Appl. Phys. Lett. **104** (2014)
Mikhailov, I.D., Garcıa, L.F., Marın, J.H.: Effect of wetting layer on electron–hole correlation in quantum discs and rings. J. Phys. Condens Matter **18**, 9493–9507 (2006)
Mobini, A., Ahmadi, V.: Design and analysis of multicolor QDIP based on metallic nanoslits array. IEEE Photonics Technol. Lett. **26**(12), 1231–1234 (2014)

Mobini, A., Solaimani, M.: A quantum rings based on multiple quantum wells for 1.2–2.8 THz detection. Physica E: Low-Dimens. Syst. Nanostruct. **101**, 162–166 (2018)
Nasri, D.: Electronic and optical properties of eccentric quantum ring under parallel magnetic field. Physica B **615**, 413077 (2021)
Nita, M., Marinescu, D.C., Manolescu, A., Ostahie, B., Gudmundsson, V.: Physica E **46**, 12 (2012)
Nunnenkamp, A., Rey, A.M., Burnett, K.: Generation of macroscopic superposition states in ring superlattices. Phys. Rev. A **77**, 023622 (2008)
Palaferri, D., Todorov, Y., Bigioli, A., Mottaghizadeh, A., Gacemi, D., Calabrese, A., et al.: Room-temperature nine-μm-wavelength photodetectors and GHz-frequency heterodyne receivers. Nature **556**, 85 (2018)
Solaimani, M., Mobini, A.: Investigation on Rashba spin-orbit interactions in two dimension quantum array for thermal imaging applications. J. Opt. **22**(8), 085001 (2020)
Solaimani, M., Izadifard, M., Arabshahi, H., Sarkardei, M.R.: J. Lumin. **134**, 699 (2013a)
Solaimani, M., Izadifard, M., Arabshahi, H., Sarkardei, M.R.: J. Lumin. **134**, 699 (2013b)
Solaimani, M., Lavaei, L., Ghalandari, M.: Intersubband optical properties of a two electron GaN/AlN constant total effective radius multi-shells quantum rings. Superlattices Microstruct. **82**, 1–10 (2015)
Splettstoesser, J., Governale, M.E., Zulicke, U.: Phys. Rev. B **68**, 165341 (2003)
Strom, N.W., Wang, Zh., Lee, J.H., AbuWaar, Z.Y., Mazur, Y., Salamo, G.J.: Nanoscale Res. Lett. 2 (2007)
Szafran, B., Bednarek, S., Dudziak, M.: Electron correlations in charge coupled vertically stacked quantum rings. Phys. Rev. B **75**, 235323 (2007)
Tan, W.-C., Inkson, J.C.: Landau quantization and the Aharonov–Bohm effect in a two-dimensional ring. Phys. Rev. B **53**, 6947 (1996)
Tomita, I., Suzuki, A.: Geometrical effect on the electron escape rate in a mesoscopic ring with an Aharonov–Bohm magnetic flux. Phys. Rev. B **53**, 9536 (1996)
Wang, X.F., Vasilopoulos, P.: Physica E 39 (2007)
Warburton, R.J., Schaflein, C., Haft, D., Blickel, F., Lorke, A., Karrai, K., Garcia, J.M., Schoenfeld, W., Petroff, P.M.: Nature (2000)
Zhu, S.-L.: Berry phase and Aharonov-Bohm effect in one-dimensional mesoscopic ring with an adiabatic rotating potential. Solid State Commun. **113**, 233–237 (2000)
Zozulenko, I.V., Maao, F.A., Hiis Hauge, E.: Quantum magnetotransport in a mesoscopic antidot lattice. Phys. Rev. B **51**(11), 7058 (1995)

Terms and Conditions

Springer Nature journal content, brought to you courtesy of Springer Nature Customer Service Center GmbH ("Springer Nature").

Springer Nature supports a reasonable amount of sharing of research papers by authors, subscribers and authorised users ("Users"), for small-scale personal, non-commercial use provided that all copyright, trade and service marks and other proprietary notices are maintained. By accessing, sharing, receiving or otherwise using the Springer Nature journal content you agree to these terms of use ("Terms"). For these purposes, Springer Nature considers academic use (by researchers and students) to be non-commercial.

These Terms are supplementary and will apply in addition to any applicable website terms and conditions, a relevant site licence or a personal subscription. These Terms will prevail over any conflict or ambiguity with regards to the relevant terms, a site licence or a personal subscription (to the extent of the conflict or ambiguity only). For Creative Commons-licensed articles, the terms of the Creative Commons license used will apply.

We collect and use personal data to provide access to the Springer Nature journal content. We may also use these personal data internally within ResearchGate and Springer Nature and as agreed share it, in an anonymised way, for purposes of tracking, analysis and reporting. We will not otherwise disclose your personal data outside the ResearchGate or the Springer Nature group of companies unless we have your permission as detailed in the Privacy Policy.

While Users may use the Springer Nature journal content for small scale, personal non-commercial use, it is important to note that Users may not:

1. use such content for the purpose of providing other users with access on a regular or large scale basis or as a means to circumvent access control;
2. use such content where to do so would be considered a criminal or statutory offence in any jurisdiction, or gives rise to civil liability, or is otherwise unlawful;
3. falsely or misleadingly imply or suggest endorsement, approval , sponsorship, or association unless explicitly agreed to by Springer Nature in writing;
4. use bots or other automated methods to access the content or redirect messages
5. override any security feature or exclusionary protocol; or
6. share the content in order to create substitute for Springer Nature products or services or a systematic database of Springer Nature journal content.

In line with the restriction against commercial use, Springer Nature does not permit the creation of a product or service that creates revenue, royalties, rent or income from our content or its inclusion as part of a paid for service or for other commercial gain. Springer Nature journal content cannot be used for inter-library loans and librarians may not upload Springer Nature journal content on a large scale into their, or any other, institutional repository.

These terms of use are reviewed regularly and may be amended at any time. Springer Nature is not obligated to publish any information or content on this website and may remove it or features or functionality at our sole discretion, at any time with or without notice. Springer Nature may revoke this licence to you at any time and remove access to any copies of the Springer Nature journal content which have been saved.

To the fullest extent permitted by law, Springer Nature makes no warranties, representations or guarantees to Users, either express or implied with respect to the Springer nature journal content and all parties disclaim and waive any implied warranties or warranties imposed by law, including merchantability or fitness for any particular purpose.

Please note that these rights do not automatically extend to content, data or other material published by Springer Nature that may be licensed from third parties.

If you would like to use or distribute our Springer Nature journal content to a wider audience or on a regular basis or in any other manner not expressly permitted by these Terms, please contact Springer Nature at

onlineservice@springernature.com